PHYSICAL REVIEW B **69**, 085316 (2004)

Modeling of type-II InAs/GaSb superlattices using an empirical tight-binding method and interface engineering

Yajun Wei* and Manijeh Razeghi†
Center for Quantum Devices, Department of Electrical and Computer Engineering, Northwestern University, Evanston, Illinois 60208, USA
(Received 14 July 2003; revised manuscript received 3 October 2003; published 20 February 2004)

We report the most recent work on the modeling of type-II InAs/GaSb superlattices using the empirical tight binding method in an sp^3s^* basis. After taking into account the antimony segregation in the InAs layers, the modeling accuracy of the band gap has been improved. Our calculations agree with our experimental results within a certain growth uncertainty. In addition, we introduce the concept of Ga_xIn_{1-x} type interface engineering in order to reduce the lattice mismatch between the superlattice and the GaSb (001) substrate to improve the overall superlattice material quality.

DOI: 10.1103/PhysRevB.69.085316 PACS number(s): 73.21.Cd, 73.61.Ey, 81.15.Hi, 85.60.Gz

INTRODUCTION

The type-II band alignment of the heterojunctions in between InAs and GaSb was first put forth by Halaski and Esaki in the 1970s.[1] Since then, high quality material growths have not been demonstrated until recent years, partially due to the growth difficulties encountered at the highly strained interfaces ($\sim 7\%$ mismatch). The quantum wells or superlattices formed by these heterojunctions are of significant potential for a wide range of applications ranging from detectors[2–5] to lasers[6,7] and modulators,[8] etc.

Important aspects of the type-II InAs/GaSb superlattice have been previously modeled using $\mathbf{k}\cdot\mathbf{p}$, pseudopotential, bond orbital, and tight-binding methods, etc. The *ab initio* calculations of the electronic structures have not been practical till now. Therefore empirical methods have become widely used. However, because the fitting parameters are highly dependent on the material quality, there has not been a universal rule that can be used consistently to explain the experimental results for superlattices grown at different conditions. In this work, we took into account a parameter that is of crucial importance during the growths: the antimony segregation in the InAs layers. With the addition of this aspect, our model can be used to explain our experimental results for superlattices grown at different growth conditions, especially the band gaps, within some growth uncertainties. With the aid of our modeling, we are also able to calculate the effects of mixed interfaces and compare with experimental results. Due to the limitation of our experimental investigation techniques, in most cases, the amount of antimony segregation remains as a general fitting parameter to a series of growths that were done using the same growth condition. It has been reported that indium and arsenic segregation exit in the GaSb layers.[9,10] However, these nonperfections are highly dependent on the details of the growth method used. We have minimized their existence through years of material growth improvements. However, because of the much lower antimony vapor pressure at a growth temperature below 400 °C compare with that above 500 °C, the residual antimony still plays an important role. The initial seeds of antimony before starting each InAs layer are significant for the material composition of the InAs layers.

EMPIRICAL TIGHT-BINDING METHOD WITH Sb SEGREGATION

The empirical tight-binding method (ETBM) originates from the early work of Slater and Koster in 1954.[11] The method was originally called linear combinations of atomic orbitals. The nonorthogonality of the atomic orbitals posed a difficulty in applying this method in an empirical frame. With the modification of the atomic orbitals to Löwdin orbitals,[12] this problem was solved. However, we assume that these orbitals still have the same symmetry as their corresponding atomic orbitals. The basis orbitals in this work should be considered only to be the Löwdin orbitals. As a balance between the modeling accuracy and the calculation load, we chose a basis of sp^3s^*, with nearest neighbor interactions, under a two-center approximation.[13,14] s^* orbitals were used to better describe the conduction bands. It can be shown that a full superlattice Hamiltonian matrix cannot be block diagonalized into two equivalent parts once the spin-orbital interactions are considered.[15] Therefore we used a full set of Löwdin orbitals with both spin-up and spin-down states in this work.

There has been significant amount of work in the theory of the ETBM for both bulk III-V materials and III-V superlattices. Here we only briefly describe the formalism to keep the integrity of this work.

Assuming the construction Lowdin orbital for the material is

$$\varphi_n^{\alpha}(\vec{r}-\vec{R}-\vec{\tau}_n),$$

where n runs through all the atoms in a unit cell, τ_n are the coordinate position vectors of the atoms in the cell, α runs though all considered types of Löwdin orbitals (s, p_x, p_y, p_z, and s^*), and R represents the coordinate position vector of the unit cell in the entire material we are considering.

The Bloch wave function of electrons for the entire material is described by

$$\Psi_{\vec{k}}(\vec{r})=\sum_{\vec{R}_{SL}}\sum_{\alpha}\sum_{n=1}^{N}\exp[i\vec{k}\cdot(\vec{R}_{SL}+\vec{\tau}_n)]$$
$$\times A_n^{\alpha}\varphi_n^{\alpha}(\vec{r}-\vec{R}_{SL}-\vec{\tau}_n),$$

 ©2004 The American Physical Society

where N is the total number of atoms in one unit cell, A_n^{α} are constants, and $\vec{R}_{SL}$ runs through all the unit cells that are involved in the nearest neighbor interactions.

The band structure calculation problem now reduces to an eigenvalue problem for $\Psi_{\vec{k}}(\vec{r})$:

$$H\Psi_{\vec{k}}(\vec{r})=E\Psi_{\vec{k}}(\vec{r}),$$

where H is the Hamiltonian operator, and E is the energy eigenvalue that is dependent on $\vec{k}$ values in the first Brillouin zone. A full description of the format for the superlattice Hamiltonian matrix is in the Appendix.

In order to better model a real superlattice that is grown with a specific technique and growth condition, we should identify important differences between a grown superlattice and an ideal superlattice. First of all, since the band gap prediction is one of the most important and fundamental tasks for any type of superlattice modeling, we will focus on this in the present work. We define an ideal type-II superlattice to be $[(\mathrm{AsIn})_m\text{-}\mathrm{AsGa}_{x1}\mathrm{In}_{1-x1}\text{-}(\mathrm{SbGa})_n\text{-}\mathrm{SbGa}_{x2}\mathrm{In}_{1-x2}]_{\mathrm{N}}$ with a perfect crystal structure, where each atomic symbol represents a layer of the same kind of atom without any exotic materials, and the sequence of atoms is exactly as it is written. Here we distinguish the interface compositions for later use. The particular atomic order we choose is only for our convenience in describing the formalism we developed, in which we start with an anion atom. In a real superlattice, first of all, at each layer which an atomic symbol represents, it is no longer the same kind in general; second, there are point defects, dislocations, etc.; third, there is always a surface miscut; fourth, the superlattice might not be perfectly periodic; fifth, the presence of the dopants would change the periodic potential. All these would make the assumption of an ideal superlattice no longer valid. Varying material parameters to accommodate these defective aspects of a real superlattice, such as band lineups at the interfaces, would not help to understand the physics behind real superlattice structures.

To model all the imperfections would be impractical as well. Fortunately, not all of these factors have the same effect on the superlattice band gap. The periodicity is a factor that can be improved with a sound practice of material growth, and we will not take into account the effects of the nonperiodicity of an actually grown superlattice. The effects of surface miscut will introduce an error bar of +/− one monolayer for each layer of InAs or GaSb, which will broaden the cutoff energy width. This is a factor that we are not considering for our superlattices in this work, since the introduced band gap error is much smaller than the band gap we are dealing with. The dislocation density can be decreased significantly by an optimization of the superlattice design with less mismatch to the substrate, which will be covered in later sections. For the point defects, there are vacancy defects, antisite defects, antimony for arsenic defects or vice versa, and dopant sites (in a general sense). Vacancy and antisite defects act as dopants, and are related to detailed growth conditions. They do not affect the band gap (unless at a high enough density that is comparable to that of the material), but rather affect the Fermi energy level in the superlattice.

TABLE I. Composition matrix for antimony segregated superlattice $[(\mathrm{AsIn})_{m-1}\text{-}\mathrm{AsGa}_{x1}\mathrm{In}_{1-x1}\text{-}(\mathrm{SbGa})_n\text{-}\mathrm{SbGa}_{x2}\mathrm{In}_{1-x2}]_{\mathrm{N}}$ within one period. $x(\mathrm{i})$ (i=1,2,...,m) represents the amount of Sb segregation. The superlattice energy terms are composition weighted arithmetic average of the corresponding materials.

Growth direction (001) ↓	Ga	In	As	Sb	
	0	0	$1-x(1)$	$x(1)$	Sb segregated InAs layers
	0	1	0	0	
	0	0	$1-x(2)$	$x(2)$	
	...	...	...	...	
	0	1	0	0	
	0	0	$1-x(m)$	$x(m)$	
	x_1	$1-x_1$	0	0	$\mathrm{Ga}_{x1}\mathrm{In}_{1-x1}$ interface
	0	0	0	1	GaSb layers
	1	0	0	0	
	...	...	...	...	
	0	0	0	1	
	1	0	0	0	
	0	0	0	1	
	x_2	$1-x_2$	0	0	$\mathrm{Ga}_{x2}\mathrm{In}_{1-x2}$ interface

The antimony for arsenic or arsenic for antimony substitution is a growth characteristic particular to type-II InAs/GaSb superlattices. We will focus on the former case in this work. This refers to the antimony segregation in the InAs layers. Due to the different properties of arsenic and antimony, only antimony segregation in the InAs layers is important. As mentioned earlier, we will not consider the indium and arsenic segregations in the GaSb layers for our superlattices.

The physical presence of the antimony segregation in the InAs layers has been reported using a scanning tunneling microscope.[16] We will follow the same notation in this work. We used the same method for the Sb segregation profile,

$$x(n)=x_i R^{n-1}(1-R)+x_0(1-R^n), \quad n=1,2,3,\ldots, \quad N_{\mathrm{InAs}}$$

where $x(n)$ stands for the composition of Sb in the nth $\mathrm{InAs}_{1-x(n)}\mathrm{Sb}_{x(n)}$ layer, x_i stands for the initial seeds of Sb, R represents the phenomenological segregation coefficient, x_0 is the Sb background incorporation ratio, and N_{InAs} stands for the number of InAs layers. A tablet description of the resulting superlattice compositions in one period is shown in Table I.

The superlattice Hamiltonian matrix is thus modified to reflect this layer dependent InAs composition using a composition weighted arithmetic average of the material parameters for InAs and InSb. For example, for the atomic section of "-$\mathrm{InAs}_{x(n)}\mathrm{Sb}_{1-x(n)}$-GaSb-," the self-interaction energy

TABLE II. The ETBM material parameters for GaAs, InAs, GaSb, and InSb at 77 K.

	GaAs	InAs	GaSb	InSb
E_{sa}	−9.2664	−9.3562	−6.0493	−9.3378
E_{sc}	−4.3504	−3.9611	−4.0712	−3.3248
E_{pa}	+1.4866	+1.8201	+0.91157	+0.39352
E_{pc}	+3.2136	+3.1842	+2.6352	+2.0791
E_{ssa}	+8.7826	+7.0432	+7.8753	+6.6378
E_{ssc}	+5.8765	+6.1232	+4.8565	+5.3807
E_{sasc}	−7.9480	−6.5393	−5.7762	−5.8320
E_{saxc}	+2.7777	+4.3607	+4.4761	+4.1129
E_{xasc}	+10.005	+7.0849	+8.2748	+7.5769
E_{ssaxc}	+3.6271	+3.0007	+5.0079	+3.4448
E_{xassc}	+7.0071	+5.4020	+6.3813	+5.8873
E_{xaxc}	+2.3069	+2.5491	+1.8244	+1.2596
E_{xayc}	+5.0305	+5.4700	+5.3733	+4.0026
Δ_a	+0.420	+0.420	+0.973	0.973
Δ_c	+0.174	+0.393	+0.174	0.393

for the $As_{x(n)}Sb_{1-x(n)}$ layer would be $\{x(n)E_{InAs}+[1-x(n)]E_{InSb}+x(n)E_{GaAs}+[1-x(n)]E_{GaSb}\}/2$, etc. The E_i (i=InAs, etc.) represents the general form for the corresponding fitting parameters. Since there exists neither common a anion nor cation between InAs and GaSb, it is important to single out the interface layers from the InAs and GaSb layers in the calculations. In order to model the real situation, a realistic model of the interface energy terms is essential. Since the superlattice layers, including the interfaces, are under high stress and strain (~7%), Harrison's d^{-2} rule[17] was also applied to scale the interaction energies. For example, at interface AsIn-As$^{(1)}$-In$^{(2)}$-Sb$^{(3)}$Ga, As$^{(1)}$ self-interaction energy would be that in a bulk InAs, that for In$^{(2)}$ would be the arithmetic average of InAs and InSb. For nearest neighbors the interaction energy between In$^{(2)}$ and Sb$^{(3)}$ would be that of InSb under stress. For a mixed interface, as another example, AsIn-As$Ga_{0.2}In_{0.8}$-SbGa, the self-interaction energy of $Ga_{0.2}In_{0.8}$ would be the arithmetic average of $Ga_{0.2}In_{0.8}As$ ($0.2E_{GaAs}+0.8E_{InAs}$) and $Ga_{0.2}In_{0.8}Sb$ ($0.2E_{GaSb}+0.8E_{InSb}$), etc. The arithmetic average scheme is adopted based on the additional characteristic of potential fields originating from different atomic sites.

The values of the ETBM parameters under the sp^3s^* nearest neighbor approximation are shown in Table II. These parameters are fitted to the known bulk band structure parameters of GaAs, InAs, GaSb, and InSb at 77 K. The band gap, spin-orbit splitting energy, effective masses at conduction band minimum and for heavy holes along the 001 direction, were fitted to the exact experimentally measured values.[18] Other band energies at high symmetry points were fitted using a numerical least squares method. The modeling results have shown that this scheme is accurate enough to predict the characteristics of the superlattices we grow. The band alignment energies between different compositional materials were from Ref. 19.

We used this modified ETBM to calculate a series of superlattices we have grown. Details of the material growths

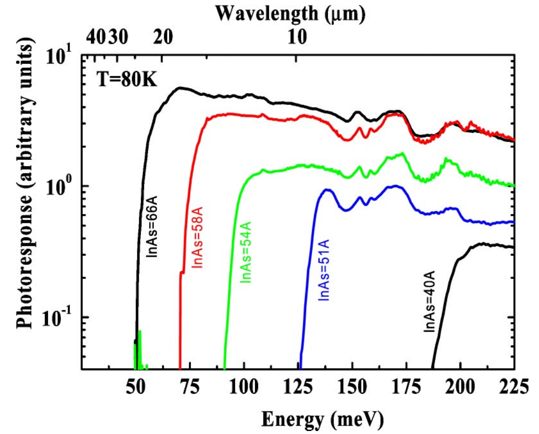

FIG. 1. (Color online) Photoresponse spectrum of a series of superlattices grown under the same condition with a fixed GaSb layer thickness of 40 Å (~13 ML) at a temperature of 80 K. The layer thickness of InAs changed from 40 Å (~13 ML) up to 66 Å (~22 ML).

have been reported elsewhere.[3–5] We fixed the GaSb layers at 40 Å (~13 ML), and varied the thickness of the InAs layers from 40 Å (~13 ML) up to 66 Å (~22 ML).[20] InSb-only interfaces were attempted for these superlattices. The experimental response spectrum of the superlattices is shown in Fig. 1. Calculations were done using fitted parameters of x_i = 0.39, x_0 = 0.012, and R = 0.67. These parameters were manually fitted to get good visual satisfaction with a reference to the values given in Ref. 16. Their accuracy is good enough to describe the whole series of superlattices for design purposes. Since each of the three parameters has its own physical meaning, the fitted numbers represents actual physical phenomena. A comparison of the calculated band gap and the experimental values is shown in Fig. 2. The calculation is in good agreement with the experimental data within certain growth uncertainties. This indicates that the ETBM is a reliable method to guide the superlattice design after considering the Sb segregation effects.

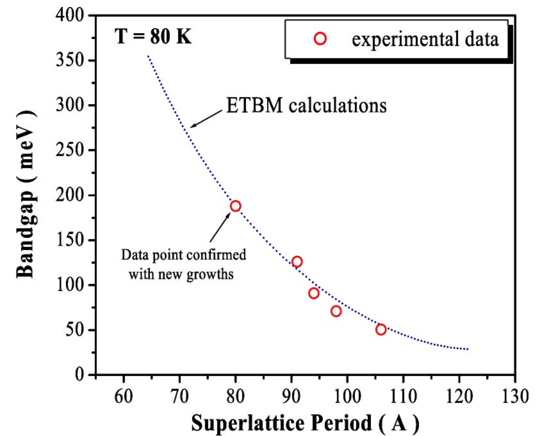

FIG. 2. (Color online) Comparison of the calculated band gap with the experimental data. The experimental data points scattered closely round the calculated curve using a modified ETBM. The cutoff wavelength for the superlattice with an InAs layer thickness of 40 Å has been confirmed with newer growths using the same growth conditions.

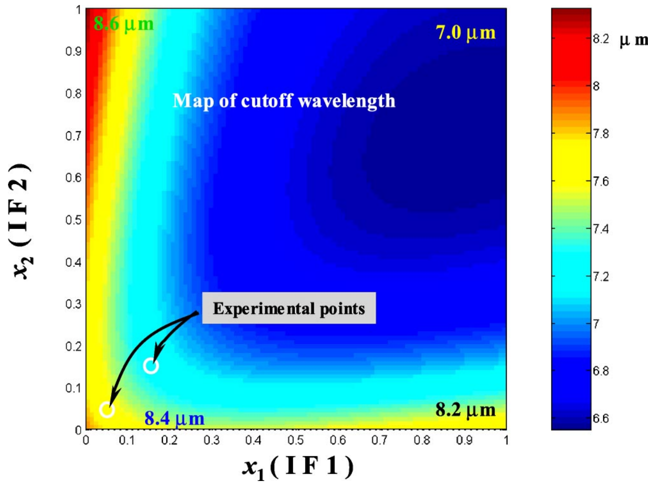

FIG. 3. (Color online) An example of calculated map of cutoff wavelengths for the superlattice of $[(\mathrm{AsIn})_{12}\text{-}\mathrm{AsGa}_{x1}\mathrm{In}_{1-x1}\text{-}(\mathrm{SbGa})_{11}\text{-}\mathrm{SbGa}_{x2}\mathrm{In}_{1-x2}]_{\mathrm{N}}$ at liquid nitrogen temperature. Notice that the two interfaces are not symmetrical. The cutoff wavelength closely depends on the interface compositions.

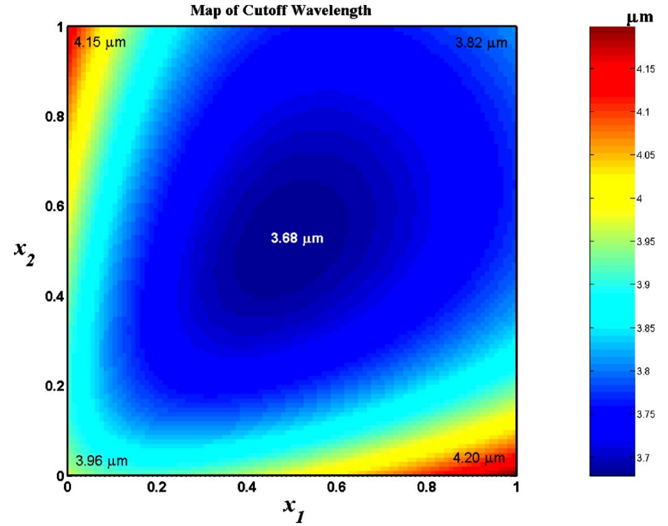

FIG. 5. (Color online) The calculated map of the cutoff wavelength for superlattice of $[(\mathrm{AsIn})_{6}\text{-}\mathrm{AsGa}_{x1}\mathrm{In}_{1-x1}\text{-}(\mathrm{SbGa})_{10}\text{-}\mathrm{SbGa}_{x2}\mathrm{In}_{1-x2}]_{\mathrm{N}}$. The cutoff wavelength variation is between 3.68 and 4.20 μm, corresponding to an energy variation of $\sim$40 meV.

INTERFACE ENGINEERING

Although it is quite obvious that the properties of type II InAs/GaSb superlattices should be strongly dependent on the interface type, only InSb and GaAs types of interfaces have been experimentally exploited before, and only $\mathrm{Sb}_x\mathrm{As}_{1-x}$ $(0<x<1)$ mixed interfaces have been theoretically investigated using the pseudopotential method.[10] By calculation, we found out that there is a certain limitation in applying only InSb or GaAs interfaces. In order to have almost zero lattice mismatches (well below 1000 ppm), there exist only a certain number of thickness combinations of InAs and GaSb (if only InSb interfaces are used) or one has to use alternating m-GaAs interfaces $(m\geqslant 0)$ with n-InSb $(n\geqslant 0, mn\neq 0)$ interfaces. For the former case, it is only valid for cutoff wavelengths greater than ~ 7 μm. Below this wavelength, there does not exist any combination of InAs and GaSb layer numbers that can satisfy the zero lattice mismatch condition. For the latter case, since the interfaces are highly strained or stressed [$\sim 7\%$ mismatch with GaSb(001) substrates], the superlattice may relax before growing the next type of interface. For the theoretically investigated $\mathrm{Sb}_x\mathrm{As}_{1-x}$ interfaces, it is not very practical to grow since the flux ratio of Sb and As is not the composition ratio of Sb and As in the material. In addition, this composition ratio is highly sensitive to the growth temperature; thus it is difficult to have good repeatability and reliability to implement this type of interface.

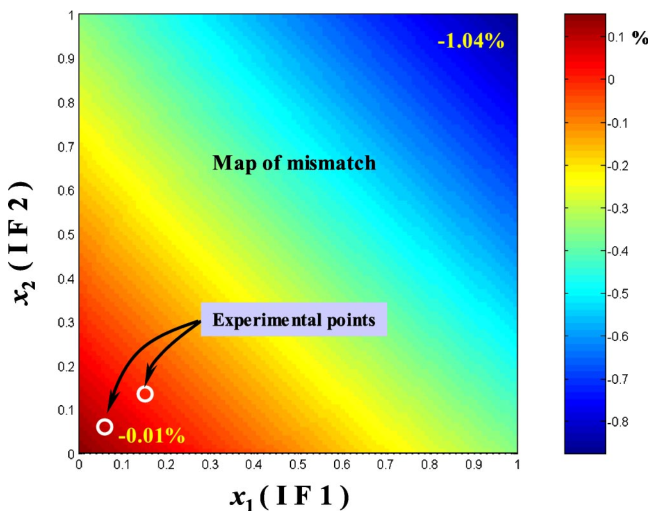

FIG. 4. (Color online) The calculated map of the lattice mismatch of the superlattice with the GaSb (001) substrate at room temperature for the superlattice of $[(\mathrm{AsIn})_{12}\text{-}\mathrm{AsGa}_{x1}\mathrm{In}_{1-x1}\text{-}(\mathrm{SbGa})_{11}\text{-}\mathrm{SbGa}_{x2}\mathrm{In}_{1-x2}]_{\mathrm{N}}$. It can be seen that the two interfaces play an identical role in affecting the lattice mismatch.

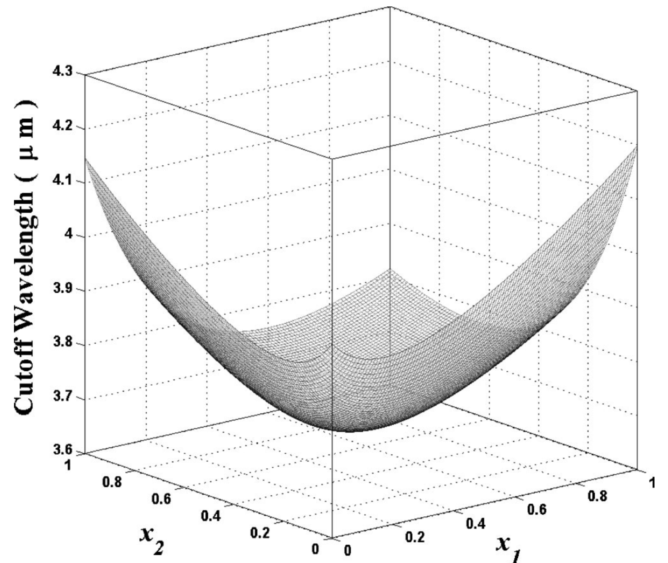

FIG. 6. The three-dimensional view of the cutoff wavelength for $[(\mathrm{AsIn})_{6}\text{-}\mathrm{AsGa}_{x1}\mathrm{In}_{1-x1}\text{-}(\mathrm{SbGa})_{10}\text{-}\mathrm{SbGa}_{x2}\mathrm{In}_{1-x2}]_{\mathrm{N}}$. The maximum cutoff wavelength can be obtained when $x_1=1$ and $x_2=0$. The minimum cutoff wavelength can be obtained when $x_1\approx 0.5$ and $x_2\approx 0.5$.

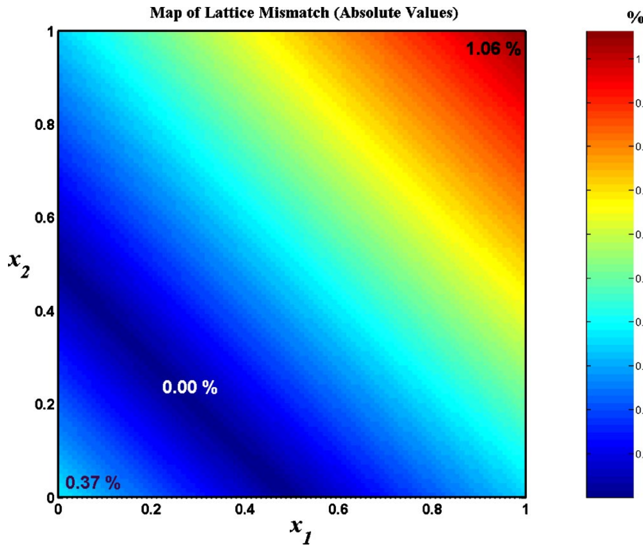

FIG. 7. (Color online) The calculated map of the absolute values for the lattice mismatch in between the superlattice of $[(\mathrm{AsIn})_6\text{-}\mathrm{AsGa}_{x1}\mathrm{In}_{1-x1}\text{-}(\mathrm{SbGa})_{10}\text{-}\mathrm{SbGa}_{x2}\mathrm{In}_{1-x2}]_\mathrm{N}$ and the GaSb (001) substrate. Significant lattice mismatch would present when using binary interfaces. We can see that within a narrow stripelike region, a zero lattice mismatch can be obtained.

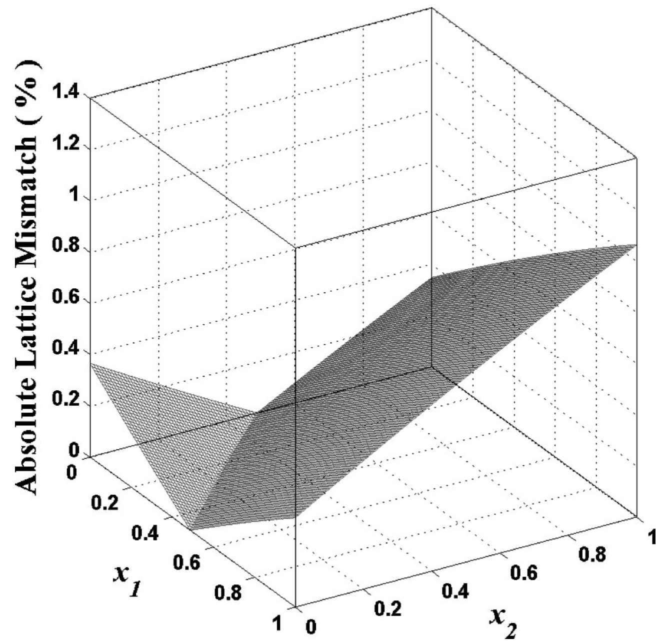

FIG. 8. The three-dimensional view of the absolute values for the lattice mismatch in between the superlattice of $[(\mathrm{AsIn})_6\text{-}\mathrm{AsGa}_{x1}\mathrm{In}_{1-x1}\text{-}(\mathrm{SbGa})_{10}\text{-}\mathrm{SbGa}_{x2}\mathrm{In}_{1-x2}]_\mathrm{N}$ and the GaSb (001) substrate. We can clearly see the zero mismatch composition line.

With these observations, we have investigated mixed interfaces of $\mathrm{Ga}_x\mathrm{In}_{1-x}$ type both theoretically using ETBM and experimentally using an Intevac Mod Gen II Molecular Beam Epitaxy system. A clear advantage of using $\mathrm{Ga}_x\mathrm{In}_{1-x}$ type interfaces is that it is highly controllable and highly repeatable because of the nonvolatility of the Ga and In species on the sample surface at a growth temperature close to 400 °C.

The calculation of the effects for this type of mixed interfaces in the ETBM is straightforward with variation of the interface compositions of x_1 and x_2. An example of a cutoff wavelength calculation at liquid nitrogen temperature for the superlattice of $[(\mathrm{AsIn})_{12}\text{-}\mathrm{AsGa}_{x1}\mathrm{In}_{1-x1}\text{-}(\mathrm{SbGa})_{11}\text{-}\mathrm{SbGa}_{x2}\mathrm{In}_{1-x2}]_\mathrm{N}$ is shown in Fig. 3. This type of superlattice has a cutoff wavelength around 8 μm at liquid nitrogen temperature. Interface No. 1 (IF 1) is denoted using $\mathrm{Ga}_{x1}\mathrm{In}_{1-x1}$ and interface No. 2 (IF 2) is denoted using $\mathrm{Ga}_{x2}\mathrm{In}_{1-x2}$. The calculated map of the cutoff wavelength reveals the nonsymmetry of IF 1 and IF 2. Only along the diagonal is the superlattice tetragonal, otherwise orthorhombic. In order to compare the calculation with the experimental values, two superlattices were grown: $[(\mathrm{AsIn})_{12}\text{-}\mathrm{AsGa}_{0.06}\mathrm{In}_{0.94}\text{-}(\mathrm{SbGa})_{11}\text{-}\mathrm{SbGa}_{0.06}\mathrm{In}_{0.94}]_\mathrm{N}$ and $[(\mathrm{AsIn})_{12}\text{-}\mathrm{AsGa}_{0.15}\mathrm{In}_{0.85}\text{-}(\mathrm{SbGa})_{11}\text{-}\mathrm{SbGa}_{0.15}\mathrm{In}_{0.85}]_\mathrm{N}$. In order to decrease the Sb segregation effects, a lower Sb flux was used for these two growths. Manually fitted segregation parameters of $x_i = 0.124$, $x_0 = 0.01$, and $R = 0.67$ were used in the calculation. Since pure GaAs interfaces will always lead to constrained superlattices (negative mismatch in the growth direction compared to the substrate) and pure InSb interfaces will always lead to compressed superlattices (positive mismatch cases), there exist certain interface composition (x_1, x_2) sets that will lead to almost zero mismatch. Figure 4 shows a calculated map of lattice mismatch with respect to the two interface compositions. It clearly shows that an almost zero mismatch can be achieved using InSb-only interfaces.

The thickness of the InAs layers needs to be decreased in order to obtain a cutoff wavelength below ~ 7 μm. If InSb-only interfaces were used, the lattice mismatch in the growth direction between the superlattice and the GaSb(001) substrate would become positive, i.e., the superlattice would begin to have a larger average lattice constant. This makes it possible to introduce Ga species into the interface layers so as to decrease the average lattice constant and balance the strain in the superlattice. As an example for superlattice of $[(\mathrm{AsIn})_6\text{-}\mathrm{AsGa}_{x1}\mathrm{In}_{1-x1}\text{-}(\mathrm{SbGa})_{10}\text{-}\mathrm{SbGa}_{x2}\mathrm{In}_{1-x2}]_\mathrm{N}$, Fig. 5 shows the calculated map of cutoff wavelength using $x_i = 0.124$, $x_0 = 0.01$, and $R = 0.67$. Figure 6 shows the three-dimensional view of the map. The entire range for x_1 and x_2 (from 0 to 1) has been calculated. We see that the cutoff wavelength can range from 3.68 to 4.20 μm, which corresponds to an energy variation of ~ 40 meV. The calculated map of mismatch (absolute values) is shown in Fig. 7, and the three-dimensional view is shown in Fig. 8. We can see clearly that there exists a zero mismatch composition line. With almost zero lattice mismatch, a superlattice of very high crystalline quality can be grown with a significant thickness in the micron range. Experimental work on the superlattice of $[(\mathrm{AsIn})_6\text{-}\mathrm{AsGa}_{0.34}\mathrm{In}_{0.66}\text{-}(\mathrm{SbGa})_{10}\text{-}\mathrm{SbGa}_{34}\mathrm{In}_{0.66}]_\mathrm{N}$ was reported in Ref. 21.

In conclusion, we have demonstrated that the ETBM is a reliable method to model the bandgap (or cutoff wavelength) of type-II InAs/GaSb superlattices after taking into account the antimony segregation factor during the superlattice growths. We also introduced the concept of $\mathrm{Ga}_x\mathrm{In}_{1-x}$-type interface engineering for a robust solution of the lattice mis-

match problem in the midwavelength infrared range 3 $\sim$7 μm, which helps to improve the overall material quality.

APPENDIX: SUPERLATTICE HAMILTONIAN MATRIX

The values of the energy terms should be those for the corresponding atoms or adjacent atomic layers. The format of the superlattice Hamiltonian is,

$$H_{\mathrm{SL}}=\begin{bmatrix} H_a & H_{ac} & 0 & 0 & \cdots & 0 & H_{ca}^{+} \\ H_{ac}^{+} & H_c & H_{ca} & 0 & \cdots & 0 & 0 \\ 0 & H_{ca}^{+} & H_a & H_{ac} & 0 & \cdots & 0 \\ 0 & 0 & H_{ac}^{+} & H_c & 0 & \cdots & 0 \\ \vdots & \vdots & 0 & 0 & \ddots & 0 & 0 \\ 0 & 0 & \vdots & \vdots & 0 & H_a & H_{ac} \\ H_{ca} & 0 & 0 & 0 & 0 & H_{ac}^{+} & H_c \end{bmatrix},$$

$$H_a=\begin{bmatrix} h_{aa} & h_{a,so} \\ h_{a,so}^{+} & h_{aa}^{*} \end{bmatrix},$$

$$h_{aa}=\begin{bmatrix} E_{sa} & 0 & 0 & 0 & 0 \\ 0 & E_{pa} & -i\frac{\Delta_a}{3} & 0 & 0 \\ 0 & i\frac{\Delta_a}{3} & E_{pa} & 0 & 0 \\ 0 & 0 & 0 & E_{pa} & 0 \\ 0 & 0 & 0 & 0 & E_{ssa} \end{bmatrix},$$

$$h_{a,so}=\begin{bmatrix} 0 & 0 & 0 & 0 & 0 \\ 0 & 0 & 0 & \frac{\Delta_a}{3} & 0 \\ 0 & 0 & 0 & -i\frac{\Delta_a}{3} & 0 \\ 0 & -\frac{\Delta_a}{3} & i\frac{\Delta_a}{3} & 0 & 0 \\ 0 & 0 & 0 & 0 & 0 \end{bmatrix}.$$

Similar forms for H_c. “*” represents complex conjugate operation, and “ $^+$” represents Hermitian conjugate operation:

$$H_{ac}=\begin{bmatrix} h_{ac} & 0 \\ 0 & h_{ac} \end{bmatrix}, \quad H_{ca}=\begin{bmatrix} h_{ca} & 0 \\ 0 & h_{ca} \end{bmatrix},$$

$$h_{ac}=\beta\cdot\begin{bmatrix} f_1E_{sasc} & \sqrt{3}f_2\cos\theta_xE_{saxc} & \sqrt{3}f_2\cos\theta_yE_{saxc} & \sqrt{3}f_1\cos\theta_zE_{saxc} & 0 \\ -\sqrt{3}f_2\cos\theta_xE_{xasc} & f_1[E_{xaxc}+(3\cos^2\theta_x-1)E_{xayc}] & 3f_1\cos\theta_x\cos\theta_yE_{xayc} & 3f_2\cos\theta_x\cos\theta_zE_{xayc} & -\sqrt{3}f_2\cos\theta_xE_{xassc} \\ -\sqrt{3}f_2\cos\theta_yE_{xasc} & 3f_1\cos\theta_y\cos\theta_xE_{xayc} & f_1[E_{xaxc}+(3\cos^2\theta_y-1)E_{xayc}] & 3f_2\cos\theta_y\cos\theta_zE_{xayc} & -\sqrt{3}f_2\cos\theta_yE_{xassc} \\ -\sqrt{3}f_1\cos\theta_zE_{xasc} & 3f_2\cos\theta_z\cos\theta_xE_{xayc} & 3f_2\cos\theta_z\cos\theta_yE_{xayc} & f_1[E_{xaxc}+(3\cos^2\theta_z-1)E_{xayc}] & -\sqrt{3}f_1\cos\theta_zE_{xassc} \\ 0 & \sqrt{3}f_2\cos\theta_xE_{ssaxc} & \sqrt{3}f_2\cos\theta_yE_{ssaxc} & \sqrt{3}f_1\cos\theta_zE_{ssaxc} & 0 \end{bmatrix},$$

$$h_{ca}=\beta\cdot\begin{bmatrix} g_1E_{sasc} & -\sqrt{3}g_2\cos\theta_xE_{xasc} & \sqrt{3}g_2\cos\theta_yE_{xasc} & \sqrt{3}g_1\cos\theta_zE_{xasc} & 0 \\ \sqrt{3}g_2\cos\theta_xE_{saxc} & g_1[E_{xaxc}+(3\cos^2\theta_x-1)E_{xayc}] & -3g_1\cos\theta_x\cos\theta_yE_{xayc} & -3g_2\cos\theta_x\cos\theta_zE_{xayc} & \sqrt{3}g_2\cos\theta_xE_{ssaxc} \\ -\sqrt{3}g_2\cos\theta_yE_{saxc} & -3g_1\cos\theta_y\cos\theta_xE_{xayc} & g_1[E_{xaxc}+(3\cos^2\theta_y-1)E_{xayc}] & 3g_2\cos\theta_y\cos\theta_zE_{xayc} & -\sqrt{3}g_2\cos\theta_yE_{ssaxc} \\ -\sqrt{3}g_1\cos\theta_zE_{saxc} & -3g_2\cos\theta_z\cos\theta_xE_{xayc} & 3g_2\cos\theta_z\cos\theta_yE_{xayc} & g_1[E_{xaxc}+(3\cos^2\theta_z-1)E_{xayc}] & -\sqrt{3}g_1\cos\theta_zE_{ssaxc} \\ 0 & -\sqrt{3}g_2\cos\theta_xE_{xassc} & \sqrt{3}g_2\cos\theta_yE_{xassc} & \sqrt{3}g_1\cos\theta_zE_{xassc} & 0 \end{bmatrix},$$

$$f_1=\frac{1}{4}[\exp(i\vec{k}\cdot\vec{\tau}_1)+\exp(i\vec{k}\cdot\vec{\tau}_2)],$$

$$f_2=\frac{1}{4}[\exp(i\vec{k}\cdot\vec{\tau}_1)-\exp(i\vec{k}\cdot\vec{\tau}_2)],$$

$$g_1=\frac{1}{4}[\exp(-i\vec{k}\cdot\vec{\tau}_3)+\exp(-i\vec{k}\cdot\vec{\tau}_4)],$$

$$g_2=\frac{1}{4}[\exp(-i\vec{k}\cdot\vec{\tau}_3)-\exp(-i\vec{k}\cdot\vec{\tau}_4)],$$

$$\vec{\tau}_1=\frac{1}{4}a_i[1+\varepsilon_{xx},1+\varepsilon_{yy},1+\varepsilon_{zz}],$$

$$\vec{\tau}_2=\frac{1}{4}a_i[-1-\varepsilon_{xx},-1-\varepsilon_{yy},1+\varepsilon_{zz}],$$

$$\vec{\tau}_3=\frac{1}{4}a_i[1+\varepsilon_{xx},-1-\varepsilon_{yy},-1-\varepsilon_{zz}],\quad \vec{\tau}_4=\frac{1}{4}a_i[-1-\varepsilon_{xx},1+\varepsilon_{yy},-1-\varepsilon_{zz}].$$

i is a material made of two adjacent atomic layers, such as InAs, InSb, GaSb, GaAs, GaInAs, GaInSb, etc. Also,

$$\beta=\frac{3}{(1+\varepsilon_{xx})^2+(1+\varepsilon_{yy})^2+(1+\varepsilon_{zz})^2},$$

$$\cos\theta_j=\sqrt{\frac{\beta}{3}}(1+\varepsilon_{jj}),\quad j=x,\ y,\ \text{or}\ z,$$

$$\varepsilon_{xx}=\varepsilon_{yy}=\frac{a_{sub}}{a_i}-1,\quad \varepsilon_{zz}=-D_i^{001}\varepsilon_{xx}.$$

a_{sub} is a substrate (GaSb) lattice constant; D_i^{001} is a strain constant of the corresponding material i.

*Email address: y-wei@northwestern.edu
†Email address: razeghi@ece.northwestern.edu

[1] G. A. Sai-Halasz, R. Tsu, and L. Esaki, Appl. Phys. Lett. **30**, 651 (1971).
[2] F. Fuchs, U. Weimer, W. Pletschen, J. Schmitz, E. Ahlswede, M. Walther, J. Wagner, and P. Koidl, Appl. Phys. Lett. **71**, 3251 (1997).
[3] H. Mohseni and M. Razeghi, Appl. Phys. Lett. **78**, 2107 (2001).
[4] Y. Wei, A. Gin, M. Razeghi, and G. J. Brown, Appl. Phys. Lett. **80**, 3262 (2002).
[5] Yajun Wei, Aaron Gin, Manijeh Razeghi, and Gail J. Brown, Appl. Phys. Lett. **81**, 3675 (2002).
[6] J. R. Meyer, C. A. Hoffman, F. J. Bartoli, and L. R. Ram-Mohan, Appl. Phys. Lett. **67**, 757 (1995).
[7] R. Q. Yang, Microelectronics J. **30**, 1043 (1999).
[8] H. Xie and W. I. Wang, J. Appl. Phys. **76**, 92 (1994).
[9] J. Steinshnider, M. Weimer, R. Kaspi, and G. W. Turner, Phys. Rev. Lett. **85**, 2953 (2000).
[10] R. Magri and A. Zunger, Phys. Rev. B **65**, 165302 (2002).
[11] J. C. Slater and G. F. Koster, Phys. Rev. **94**, 1498 (1954).
[12] P. Löwdin, J. Chem. Phys. **18**, 365 (1950).
[13] P. Vogl, Harold P. Hjalmarson, and John D. Dow, J. Phys. Chem. Solids **44**, 365 (1983).
[14] D. N. Talwar, John P. Loehr, and B. Jogai, Phys. Rev. B **49**, 10 345 (1994).
[15] L. C. Lew Yan Voon, Ph.D. thesis, WPI, Worcester, MA, 1993.
[16] J. Steinshnider, J. Harper, M. Weimer, C. H. Lin, S. S. Pei, and D. H. Chow, Phys. Rev. Lett. **85**, 4562 (2000).
[17] Walter A. Harrison, *Electronic Structure and the Properties of Solids: The Physics of the Chemical Bond* (Dover, New York, 1989), ISBN: 0-486-66021-4.
[18] O. Madelung, W. von der Osten, and U. Rössler, in *Numerical Data and Functional Relationships in Science and Technology*, edited by O. Madelung and M. Schulz, Landolt-Börnstein New Series, Group III, Vol. 22, Pt. a (Springer-Verlag, New York/Heidelberg/Berlin, 1987), ISBN: 0-387-16609-2.
[19] Chris G. Van de Walle, Phys. Rev. B **39**, 1871 (1989).
[20] H. Mohseni, Y. Wei, and M. Razeghi, Proc. SPIE **4288**, 191 (2001).
[21] Yajun Wei, Junjik Bae, Aaron Gin, Andrew Hood, Manijeh Razeghi, Gail J. Brown, and Meimei Tidrow, J. Appl. Phys. **94**, 4720 (2003).